

## CHAPTER 88

### NEARFIELD TSUNAMIS GENERATED BY THREE DIMENSIONAL BED MOTIONS

J.J. Lee\* & J.J. Chang\*\*

#### ABSTRACT

A theoretical and computer simulation has been conducted on near field tsunamis generated by three dimensional bed motion. Linear dispersive wave theory has been used. Nonlinear effect has been found to be negligible for nearfield tsunami generation problem, as nonlinear effect is significant primarily for propagation over long distances. The specified bed deformation takes into account many possible dipole dislocation patterns with different aspect ratio. Three dimensional pictures of the water surface elevation were constructed from the array of computer data.

For the nearfield tsunamis problem, the distance between the generation area and the shoreline is relatively short, thus the main generated wave quickly interact with the reflected leading wave from the coastal boundary to create an even more complicated wave profile. The coastal boundary can either focus or diffuse these waves, resulting in large variations in wave amplitude in the coastal region.

#### (I) PROBLEM FORMULATION

Let  $(x, y, z)$  constitute a Cartesian coordinate system with  $z = 0$  as the undisturbed water surface as shown in Fig. 1. Initially, the fluid is at rest with the free surface and solid boundary defined by  $z = 0$  and  $z = h$  respectively, where  $h$  is a constant. For  $t > 0$ , the solid boundary is moved as prescribed by  $\xi(x, y; t)$ . The resulting deformation of the free surface is to be determined as  $z = \eta(x, y; t)$ . Assuming irrotational flow and an inviscid

---

\* Jiin-Jen Lee, Professor of Civil Engineering, Department of Civil Engineering, University of Southern California, Los Angeles, CA 90089-2531

\*\* John J. Chang, President of John Chang & Associates, 1116 Loganrita Ave., Arcadia, CA 91006 (Formerly, Research Engineer in Civil Engineering, University of Southern California, Los Angeles, CA 90089-2531).

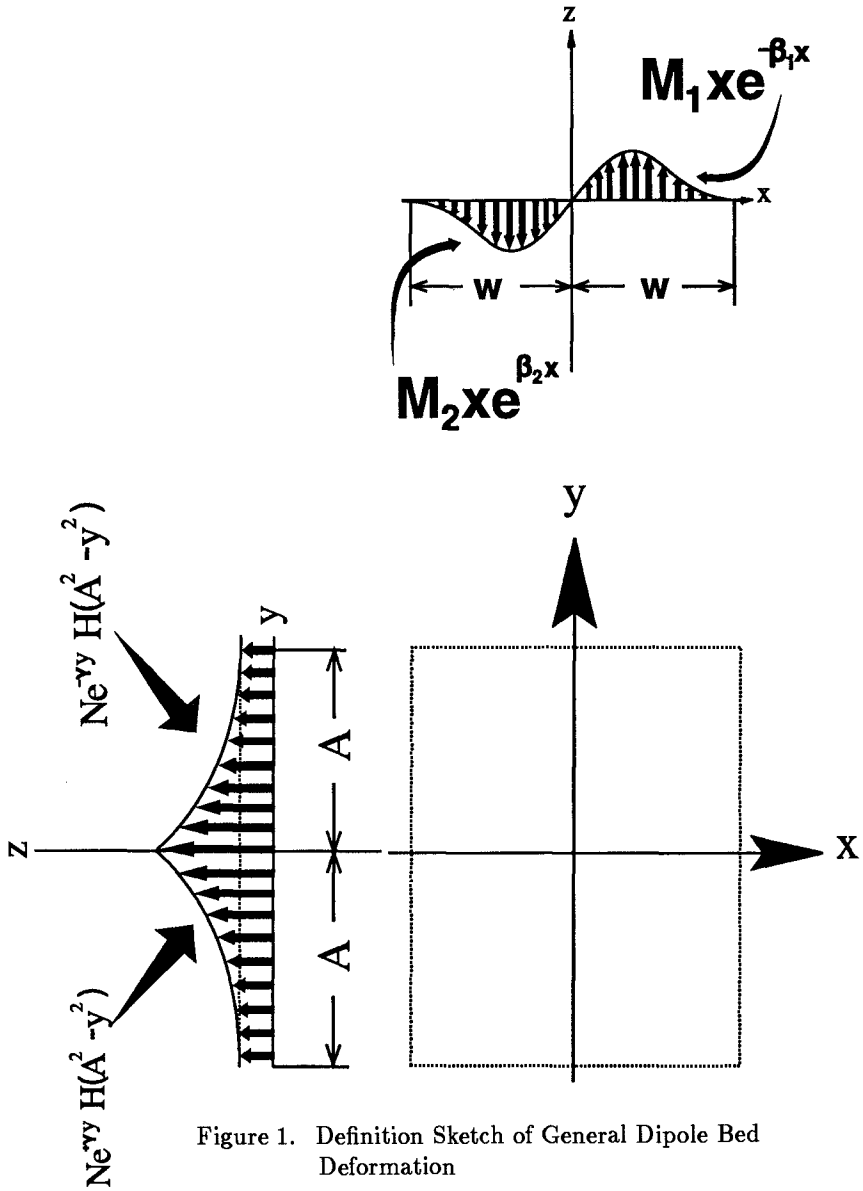


Figure 1. Definition Sketch of General Dipole Bed Deformation

fluid, the fluid kinematics can be expressed in terms of a velocity potential  $\varphi(x, y, z; t)$ . The differential equation and the linearized boundary conditions that  $\varphi$  must satisfy can be listed as follows:

$$\Delta^2 \varphi = 0 \quad 0 < t < \infty, -\infty < x, y < \infty, -h < z < 0 \quad (1)$$

$$\varphi_{tt} + g\varphi_z = 0 \quad z = 0 \quad (2)$$

$$\varphi_z = \xi(x, y; t) \quad z = -h \quad (3)$$

In these equations, the subscripts denote partial derivatives and  $g$  denotes the gravitational acceleration.

The linearized relation between the water surface displacement,  $\eta$ , and the velocity potential,  $\varphi$ , is

$$\eta(x, y; t) = -\frac{1}{g}\varphi_t(x, y, 0; t) \quad (4)$$

The solution for  $\varphi$  (and hence,  $\eta$ ) is obtained by using the Fourier transform for the spatial variables  $x, y$  and the Laplace transform for the time variable  $t$  defined by:

$$\hat{f}(K_1, K_2, s) = \int_0^\infty e^{-st} \int_{-\infty}^\infty e^{iK_2 y} \int_{-\infty}^\infty e^{iK_1 x} f(x, y; t) dx dy dt \quad (5)$$

By applying the transformation of equation (5) to the governing equation and boundary conditions with the subsequent inversion, one obtains the water surface elevation as:

$$\eta(x, y; t) = \frac{1}{(2\pi)^2} \int_{-\infty}^\infty \int_{-\infty}^\infty \left[ \frac{1}{2\pi i} \int_{B_\gamma} \frac{s^2 e^{-iK_1 x} e^{-iK_2 y} e^{st} \hat{\xi}(K_1, K_2, s)}{(s^2 + \omega^2) \cosh \sqrt{K_1^2 + K_2^2} h} ds \right] dK_1 dK_2 \quad (6)$$

where  $\omega^2 = g\sqrt{K_1^2 + K_2^2} \tanh \sqrt{K_1^2 + K_2^2} h$  and  $\int_{B_\gamma} \equiv \lim_{\Gamma \rightarrow \infty} \int_{\mu - i\Gamma}^{\mu + i\Gamma}$  is the Bromwich constant,  $\mu$  is a positive constant and  $\Gamma$  is a real number.

In order to obtain the specific wave profile as defined in equation (6), one must specify the bed deformation history  $\xi(x, y; t)$ . The bed deformation is assumed to be a rectangular block with a dipole type of deformation in  $x$  axis, and exponential variation in time:

$$\xi(x, y; t) = T(t)X(x)Y(y) \quad (7)$$

where

$$\begin{aligned}
 T(t) &= \xi_0(1 - e^{-\alpha t}) \quad t \geq 0 \\
 X(x) &= \begin{cases} M_1 x e^{-\beta_1 x} & x \geq 0 \\ M_2 x e^{\beta_2 x} & x < 0 \end{cases} \\
 Y(y) &= N e^{-\gamma|y|} H(A^2 - y^2)
 \end{aligned}$$

$\xi_0$  is the maximum amplitude of the vertical displacement,  $\alpha$  is the time constant defined as  $1.11/t_c$ , and  $t_c$  is the characteristic time defined by  $\xi/\xi_0 = 2/3$  at  $t = t_c$ .  $M_1$ ,  $M_2$ ,  $\beta_1$  and  $\beta_2$ , are real and positive constant,  $A$  is a half length of the rectangular block. The heavy side step function is defined as:

$$H(A^2 - y^2) = \begin{cases} 1, & A^2 - y^2 > 0 \\ 0, & A^2 - y^2 < 0. \end{cases}$$

The transformation of equation (7) yields:

$$\begin{aligned}
 \hat{\xi}(K_1, K_2; s) &= \left\{ M_1 \left[ \frac{\beta_1^2 - K_1^2 + 2i\beta_1 K_1}{(\beta_1^2 + K_1^2)^2} \right] \right. \\
 &\quad \left. - M_2 \left[ \frac{\beta_2^2 - K_1^2 + 2i\beta_2 K_2}{(\beta_2^2 + K_1^2)^2} \right] \right\} 2Ni. \\
 &\quad \left\{ \frac{e^{-\gamma A}}{\gamma^2 + K_2^2} [-\gamma \cos K_2 A + K_2 \sin K_2 A] + \frac{\gamma}{\gamma^2 + K_2^2} \right\} \cdot \\
 &\quad \xi_0 \left[ \frac{\alpha}{s(s + \alpha)} \right]
 \end{aligned} \tag{8}$$

Substituting equation (8) into equation (6) and solving for the surface elevation one obtains:

$$\begin{aligned}
 \eta(x, y; t) &= \frac{-2\xi_0 Ni}{(2\pi)^2} \int_{-\infty}^{\infty} \int_{-\infty}^{\infty} \left\{ M_1 \left[ \frac{\beta_1^2 - K_1^2 + 2i\beta_1 K_1}{(\beta_1^2 + K_1^2)^2} \right] \right. \\
 &\quad \left. - M_2 \left[ \frac{\beta_2^2 - K_2^2 + 2i\beta_2 K_2}{(\beta_2^2 + K_1^2)^2} \right] \right\} \cdot \\
 &\quad e^{-iK_1 x} \cdot \left\{ \frac{e^{-\gamma A}}{\gamma^2 + K_2^2} [-\gamma \cos K_2 A + K_2 \sin K_2 A] + \frac{\gamma}{\gamma^2 + K_2^2} \right\} \cdot e^{-iK_2 y} \cdot \\
 &\quad \frac{1}{\cosh \sqrt{K_1^2 + K_2^2} h} \cdot \left[ \frac{\alpha^2}{\alpha^2 + \omega^2} (e^{-\alpha t} - \cos \omega t - \frac{\omega}{\alpha} \sin \omega t) \right] dK_1 dK_2
 \end{aligned}$$

where

$$\omega^2 = g \sqrt{K_1^2 + K_2^2} \tanh \sqrt{K_1^2 + K_2^2} h \tag{9}$$

To obtain a simplified solution from equation (9) the bed deformation is assumed to be axially symmetrical. A sketch of such specific fluid domain is

set in Fig. 1 for the case of  $M_1 = M_2 = M$ ,  $\beta_1 = \beta_2 = \beta$ ,  $\gamma = 0$  and  $N = 1$ . Thus, equation (9) becomes:

$$\eta(x, y; t) = \frac{2\xi_0\beta M}{\pi^2} \int_{-\infty}^{\infty} \int_{-\infty}^{\infty} \frac{\sin K_2 A}{K_2} \frac{K_1}{(\beta^2 + K_1^2)^2} \cdot e^{-iK_1 x} \cdot e^{-iK_2 y} \cdot \frac{1}{\cosh \sqrt{K_1^2 + K_2^2} h} \left[ \frac{\alpha^2}{\alpha^2 + \omega^2} (e^{-\alpha t} - \cos \omega t - \frac{\omega}{\alpha} \sin \omega t) \right] dK_1 dK_2$$

where

$$\omega^2 = g\sqrt{K_1^2 + K_2^2} \tanh \sqrt{K_1^2 + K_2^2} h \quad (10)$$

Equation (10) contains poles at  $K_2 = 0$ . This singularity can be treated easily by  $L'$  Hospital's rule.

Introducing  $K_1 = -2\pi k_1$  and  $K_2 = -2\pi k_2$ , equation (10) can be rewritten as:

$$\eta(x, y; t) = 8\beta M \xi_0 \int_{-\infty}^{\infty} \int_{-\infty}^{\infty} e^{i2\pi k_1 x} e^{i2\pi k_2 y} f(k_1, k_2) dk_1 dk_2 \quad (11)$$

where

$$f(k_1, k_2) = \frac{-2\pi k_1}{[\beta^2 + (2\pi k_1)^2]^2} \cdot \frac{\sin 2\pi k_2 A}{2\pi k_2} \cdot \frac{1}{\cosh \sqrt{(2\pi k_1)^2 + (2\pi k_2)^2} h} \left[ \frac{\alpha^2}{\alpha^2 + \omega^2} (e^{-\alpha t} - \cos \omega t - \frac{\omega}{\alpha} \sin \omega t) \right]$$

and

$$\omega^2 = g\sqrt{(2\pi k_1)^2 + (2\pi k_2)^2} \tanh \sqrt{(2\pi k_1)^2 + (2\pi k_2)^2} h$$

It should be recognized that equation (11) is a two dimensional Fourier transform of  $f(k_1, k_2)$ , and can be computed by using the fast Fourier transform (FFT).

## (II) NUMERICAL IMPLEMENTATION

Suppose that  $f(k_1, k_2)$  is defined in the interval of  $-T/2 < k_1, k_2, \frac{T}{2}$  and is zero for  $|k_1|, |k_2| > T/2$ , equation (11) can then be written as:

$$\eta(x, y; t) = 8\beta M \xi_0 \int_{-\frac{T}{2}}^{\frac{T}{2}} \int_{-\frac{T}{2}}^{\frac{T}{2}} e^{i2\pi k_1 x} e^{i2\pi k_2 y} f(k_1, k_2) dk_1 dk_2 \quad (12)$$

It should be noted that the advantageous procedure of computing  $\eta(x, y; t)$  in equation (12) is to fix a time  $t = t_i$  and evaluate all possible  $x$  and  $y$  by recognizing equation (12) as a double Fourier transform of  $f(k_1, k_2; t)$ .

The integral in equation (12) can be approximated by Reimann sum. Thus, equation (12) became as two-dimensional discrete Fourier Transform form:

$$\eta(k_1, k_2; t) = 8\beta M \xi_0 \Delta k_1 \Delta k_2 \sum_{n_1 = -\frac{N_1}{2} + 1}^{N_1/2} \sum_{n_2 = -\frac{N_2}{2} + 1}^{N_1/2} f(n_1, n_2) \omega_1^{k_1 n_1} \omega_2^{k_2 n_2}$$

$$\text{for } \frac{-N_1}{2} + 1 \leq k_1 \leq \frac{N_1}{2}, \quad \frac{-N_2}{2} + 1 \leq k_2 \leq \frac{N_2}{2} \quad (13)$$

where

$$f(n_1, n_2) = \frac{-2\pi n_1 \Delta k_1}{[\beta^2 + (2\pi n_1 \Delta k_1)^2]^2} \cdot \frac{\sin 2\pi n_2 \Delta k_2 A}{2\pi n_2 \Delta k_2} \cdot \frac{1}{\cosh \sqrt{(2\pi n_1 \Delta k_1)^2 + (2\pi n_2 \Delta k_2)^2} h} \cdot \left[ \frac{\alpha^2}{\alpha^2 + \omega^2} (e^{-\alpha t} - \cos \omega t - \frac{\omega}{\alpha} \sin \omega t) \right],$$

and

$$\omega^2 = g \sqrt{(2\pi n_1 \Delta k_1)^2 + (2\pi n_2 \Delta k_2)^2}$$

$$\tanh \sqrt{(2\pi n_1 \Delta k_1)^2 + (2\pi n_2 \Delta k_2)^2} h$$

$N_1$  and  $N_2$  are the number of discrete points which correspond to the  $x$  and  $y$  axis, respectively;  $n_i = -\frac{N_i}{2} + 1, -\frac{N_i}{2} + 2, \dots, \frac{N_i}{2}$  for  $i = 1, 2$ . The constant length,  $\Delta k_i = 2T/N_i$  for  $i = 1, 2$ . This definition of  $\Delta k_i$ , implies that  $\Delta x = \Delta y = \frac{1}{2T}$ , and  $x = k_1 \cdot \Delta x, y = k_2 \cdot \Delta y$ .

It should be noted that  $\omega_1 = e^{2\pi i/N_1}$  and  $\omega_2 = e^{2\pi i/N_2}$  introduced in equation (13) are  $N_1 - th$  and  $N_2 - th$  roots of unity in the complex number field, respectively.

An array of  $256 \times 256$  points was used to compute equation (13), i.e.  $N_1 = N_2 = 256$  and  $m = 8$ . To avoid the spurious short-period oscillations,  $\Delta k$  should be kept small. However, a small  $\Delta k$  implies that the region of computation is also correspondingly limited. All numerical results presented in this study are obtained for  $\Delta k = 0.03$ . This value was arrived at through a series of numerical experiments.

In order to obtain the wave profile as defined in equation (13), one must specify the parameters  $M$  and  $\beta$ , for the comparison study, the results

obtained for the water wave generated by equation (13) will be compared with the previously published half-sine type dipole dislocation results (Chang (1981)). It should be noted that the bed deformation of half-sine type dipole dislocation is also assumed to be rectangular block with a dipole type of deformation in  $x$ -axis and exponential variation in time. This is specified as follows:

$$\xi(x, y; t) = \xi_0(1 - e^{-\alpha t})\left(\sin \frac{\pi x}{2B}\right)[H(B^2 - x^2)H(A^2 - y^2)]. \quad (14)$$

In order to set the resulting bed deformation specified by equation (7) and (14) to have the the same deformation energy as well as the same displacement volume the parameter  $M$  is equal to 5.8 and  $\beta$  is equal to 2.134.

### (III) RESULTS AND DISCUSSION

Numerical results obtained from equation (13) for a general case dipole dislocation of a rectangular block have been obtained. A series of three-dimensional pictures of the wave surface elevation are presented in figure 2 for different dimensionless time parameters,  $t\sqrt{g/h}$ . The dimensionless parameters for this case are:  $t_c\sqrt{g/h}/B = 0.069$ ,  $B/h = 12.2$  ( $B$  is the effective half width of a rectangular block, let  $B = \frac{1}{2}W = 2.0$  as shown in Fig. 1),  $\xi_0/h = 0.2$ . The time history of bed motion is an exponential form as seen in Equation (7) with a characteristic time parameter,  $\alpha = 18.46$ . These three-dimensional pictures were constructed from  $256 \times 256$  pixel using image processing technique, and represent the overall pictorial view of the wave profile at  $t\sqrt{g/h} = 4.20, 12.61, 21.02$  and  $29.43$ . The vertical viewing angle for these pictures is  $60^\circ$  and the horizontal angle is  $60^\circ$ . The wave amplitude,  $\eta$ , has been normalized by the total bed displacement,  $\xi_0$ . By inspecting these three-dimensional pictures the wave along the  $x$ -axis are transformed from the original exponential form into waves of two opposite directions outward from the generation region. The waves along the  $y$ -axis disperse from the original wave form as time increase. Due to radiation of wave in every direction, the extent of the generated regions are presented as approximately elliptic region. The complex nature of generated wave patterns due to three-dimensional bottom dislocation is shown in these pictures.

In order to demonstrate the transformation of wave profile as a function of time, the water surface profile along any arbitrarily chosen coordinates by a generalized digital mathematical phantom is also obtained. Figure 3 show the water surface profile along  $x$  axis ( $y = 0$  for  $x > 0$ ). For convenient comparison of the results for the two different bed motion.

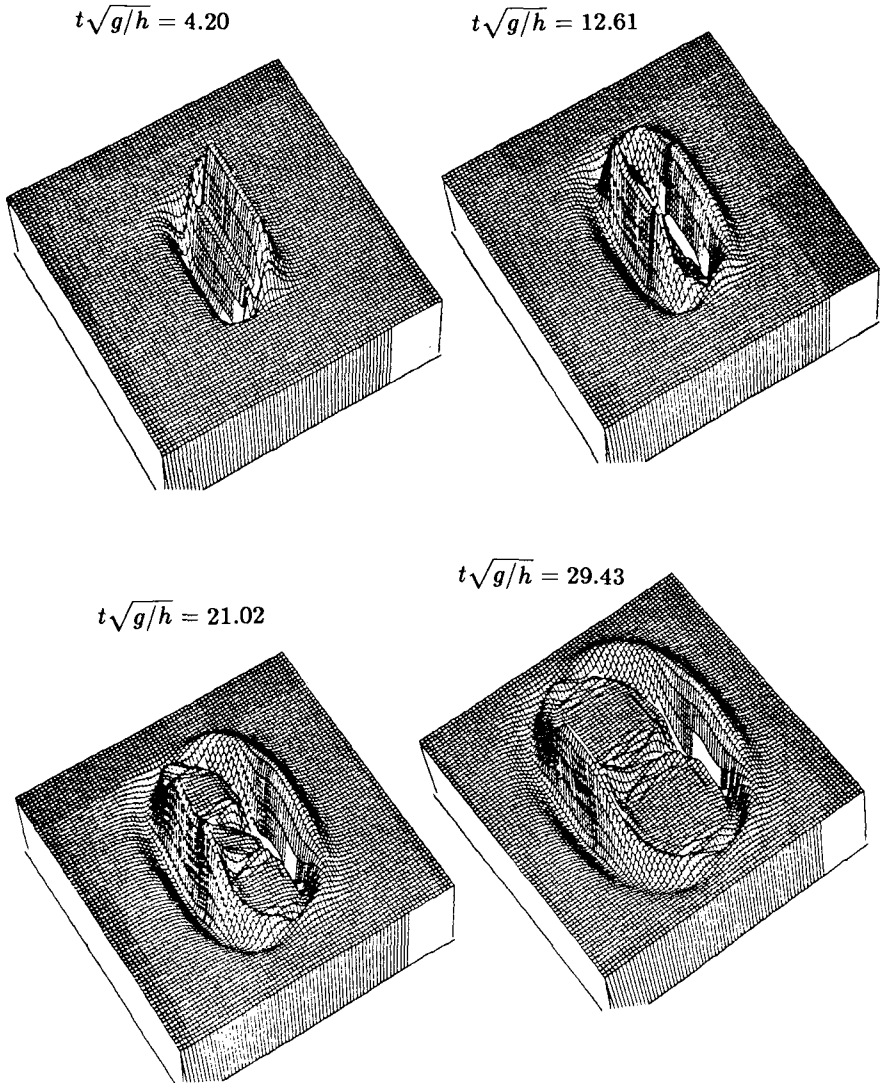


Figure 2. Three Dimensional Pictures Due to General Case Dipole Dislocation Bed Motion Showing the Wave Pattern Near the Generation Region for Specified Time Parameters (Viewing Angle:  $\theta_h = 60^\circ$ ,  $\theta_v = 60^\circ$ )

The water profiles for a half-sine type dipole dislocation are also superimposed in Figures 3. These profiles are obtained by cutting the three-dimensional pictures such that shown in Figure 2. This series of water surface profiles shows how detailed waves are propagated from the origin of disturbance towards the surrounding region. By studying these wave profiles at different time parameters for both types of bed motion as shown in Figures 3, a number of observations can be made:

- (a) The limit of undisturbed water surface is consistent for all time parameters, even when the bottom disturbances differ.
- (b) The water surface profiles for both dipole bed motions obtained, show an asymmetric behavior due to the asymmetric bottom deformation. The wave amplitude along the  $y$ -axis is also zero at all the time. It should be noted that the present theoretical analysis does not treat the nonlinear effect, although the dispersive effect is allowed. Using these wave profiles, the propagation speed is also computed as 2.2 ft/sec, this is very close to the longwave celerity  $c = \sqrt{gh} = 2.3$  ft/sec.
- (c) At a small time parameter,  $t\sqrt{g/h} = 8.41$ , the wave profiles due to general case dipole dislocation differ from the wave patterns due to the half-sine type dipole dislocation. This has provided an aspect showing the end effect of the generation region arriving at the  $x$ -axis. The generated wave profiles are dependent upon the shape of bed motion.
- (d) For the general type dipole dislocation, the wave amplitude decay rapidly in arbitrary direction (see Figures 3) the rate of decay is faster than the case of half-sine dipole dislocation the wave profiles exhibited larger negative wave trailing the positive leading wave.

The water surface profiles for two different bed deformations as a function of time at three locations away from the generated region are shown in Figure 4. The three locations are chosen along the minor axis ( $y = 0$ ) at  $x = 1.5B$ ,  $2.0B$  and  $2.5B$ . It is seen that the wave profiles in these three locations shows the same time of arrival for different bed motion. The negative leading wave trailing the positive wave propagates away from the generation region, and oscillates in a manner which appears to be approaching the still water surface level as time increase. For the case of general dipole dislocation the negative leading wave trailing the positive wave occurs at a smaller value of  $t\sqrt{g/h}$ , than that for the case of half-sine bed motion.

To demonstrate the effect of coastal boundary on the nearfield tsunamis generated by the current bed motion models eight computer graphics are presented in Figure 5. These computer graphics show wave patterns for various time after the start of the bed motion as they approach the coastal boundary. The orientation of the coastal boundary is inserted in Figure 5. The computer graphics are generated by different viewing angles providing the

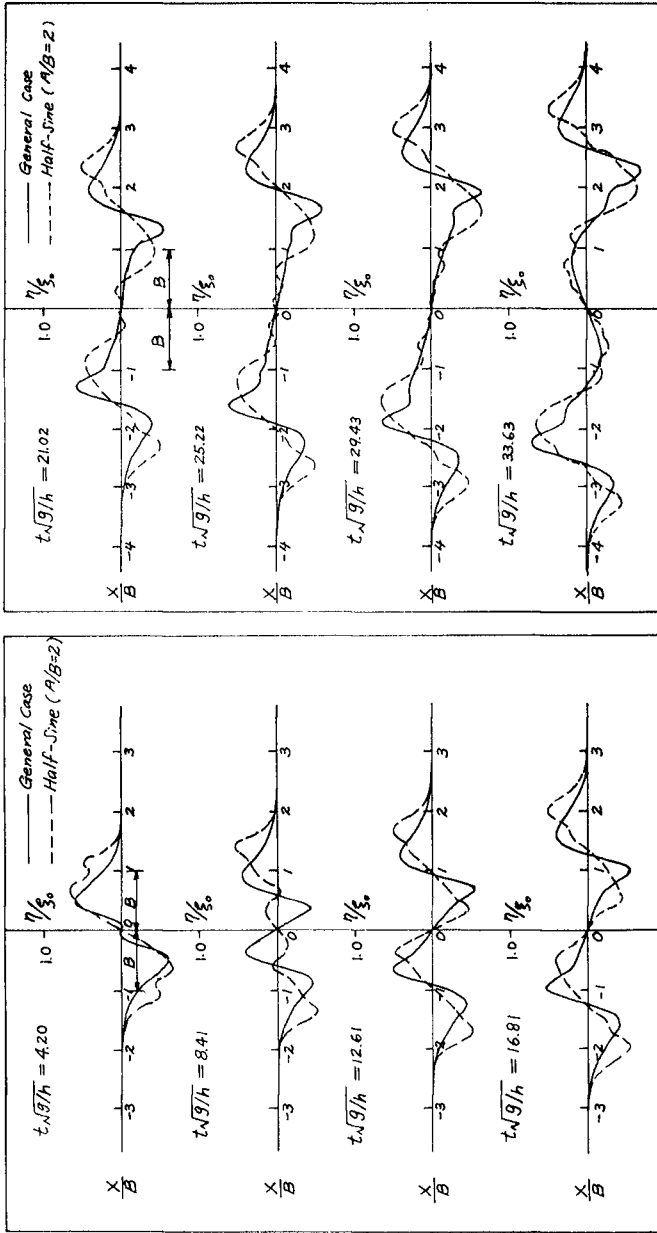


Figure 3. Water Surface Profile Along the x-Axis for Two Different Bed Deformation Models

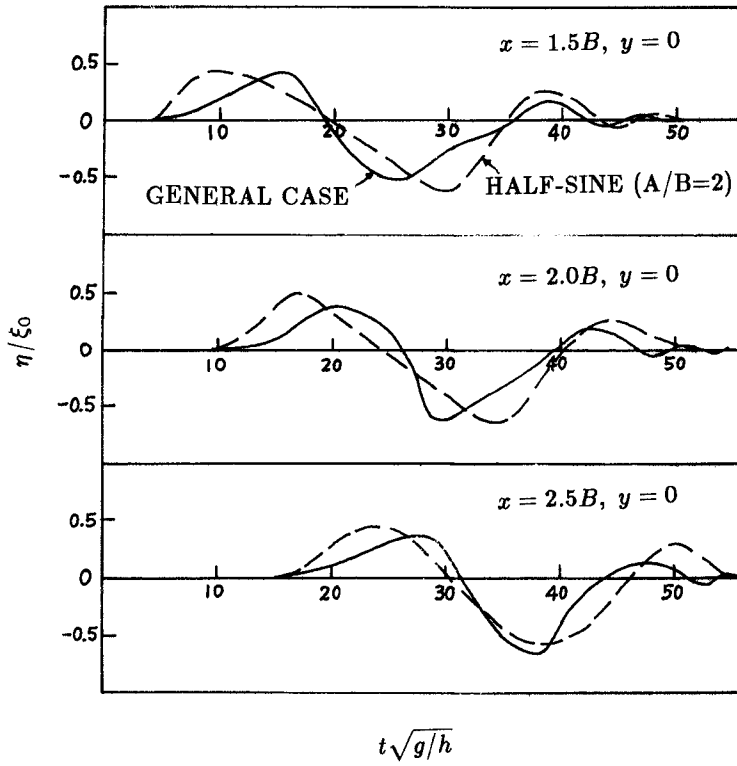


Figure 4. Water Surface Profiles for Two Different Bed Deformation Models at  $x = 1.5B, 2.0B$ , and  $2.5B; y = 0$

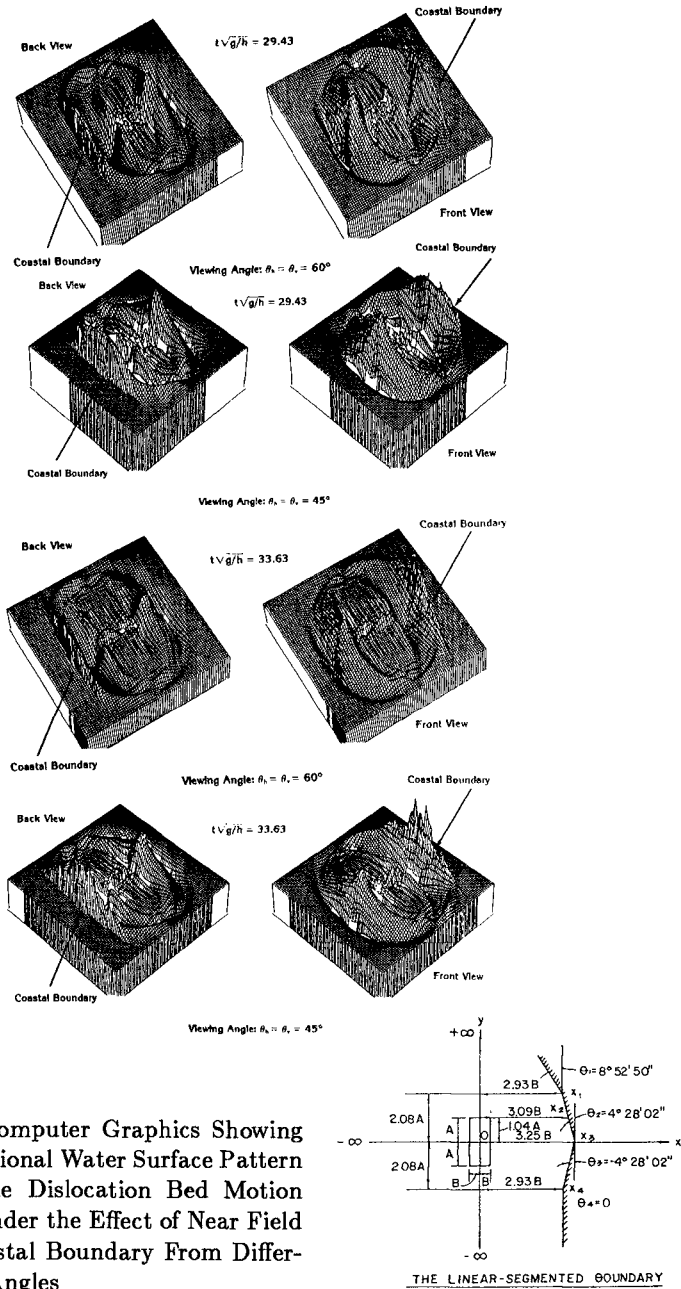


Figure 5. Computer Graphics Showing Three Dimensional Water Surface Pattern Due to Dipole Dislocation Bed Motion ( $A/B = 2$ ) Under the Effect of Near Field Irregular Coastal Boundary From Different Viewing Angles

wave pattern from different perspective. From these, one can readily see the effect of the reflecting boundary and realize the variation of the transient wave amplitudes along the coastal boundary associated with nearfield tsunamis. This feature confirms the field experience which showed a great variation in wave amplitudes at nearby locations along the coastline. It should be noted that the water depth throughout the computational domain has been assumed constant. The resulting water surface profile for variable depth medium would even be more complicated than those shown.

## REFERENCES

1. Andrews, H.C., *Computer Techniques in Image Processing*, Academic Press, New York, 1970.
2. Brigham, E.O., *The Fast Fourier Transform*, Prentice-hall, Inc., Englewood Cliffs, New Jersey, 1974.
3. Chang, J.J., "Water Wave Generated by Three-Dimensional Bed Motion," *Ph.D. Dissertation*, University of Southern California, Dec., 1981.
4. Driessche, P.V.D., and Braddock, R.D., "On the Elliptic Generating Region of a Tsunami," *Journal of Marine Research*, Australia, 1972, pp. 217-226.
5. Hammach, J.L., "A Note on Tsunamis: Their Generation and Propagation in an Ocean of Uniform Depth," *Journal of Fluid Mechanics*, Vol. 60, Part IV, 1973, pp. 769-799. (For more details, see Report No. KH-R-28, W.M. Keck Laboratory of Hydraulics and Water Resource, California Institute of Technology, Pasadena, CA, 1972.)
6. Kajiura, K., "Tsunami Source, Energy and the Directivity of Wave Radiation," *Bulletin of the Earthquake Research Institute*, Tokyo University, Vol. 48, 1970, pp. 835-869.
7. Lee, J.J., and Chang, J.J., "Wave Generated by an Impulsive Bed Motion of Finite Size," *Proceeding of the Second Congress of the Asian and Pacific Regional of IAHR*, International Conference on Water Resources Development, Taipei, Taiwan, 12-14 May 1980, pp. 759-768.
8. Lee, J.J., and Chang, J.J., "Water Waves Generated by an Impulsive Bed Upthrust of a Rectangular Block," *Applied Ocean Research*, Vol. 2, NO. 4, 1980, pp. 165-170.
9. Oppenheim, A.V., and Schafer, R.W., *Digital Singal Processing*, Prentice-Hall, Inc., Englewood Cliffs, NJ, 1975.

10. Reed, I.S., Glenn, W.V. Jr., Truong, T.K., Kwoh, Y.S., and Chang, C.M., "X-Ray Reconstruction of the Spinal Cord, Using Bone Suppression, Appendix I and III," *IEEE Transactions on Bio-medical Engineering*, Vol. BME-27, No. 6, 1980, pp. 293-298.
11. Sabatier, Pierre C., "Formation of Wave by Ground Motion" Chapter 17 of *Encyclopedia of Fluid Mechanics*, Gulf Publishing Company, 1986, pp. 723-759.
12. Van Dorn, W.G., "Tsunamis," *Advances in Hydroscience*, Vol. 2, 1965, pp. 1-48.